PAPER

Topological phase transition at the interface of a topological with a conventional insulator

IOP Publishing Journal of Physics: Condensed Matter
J. Phys.: Condens. Matter **32** (2020) 235001 (11pp) https://doi.org/10.1088/1361-648X/ab70c2

Topological phase transition at the interface of a topological with a conventional insulator

Niraj Aryal[1] **and Efstratios Manousakis**[1,2]

[1] Department of Physics and National High Magnetic Field Laboratory, Florida State University, Tallahassee, FL 32306-4350, United States of America
[2] Department of Physics, University of Athens, Panepistimioupolis, Zografos, 157 84 Athens, Greece

E-mail: aryalniraj7@gmail.com and manousakis@gmail.com

Received 15 October 2019, revised 5 January 2020
Accepted for publication 28 January 2020
Published 10 March 2020

Abstract

We study the topological states which appear at the interface between a topological insulator (TI) and a conventional insulator (CI) using effective Hamiltonians which accurately describe the band structure of the Bi_2Se_3 family. Due to the hybridization between the TI and the CI states, the band-gap that appears in the interface Dirac cone decreases and ultimately vanishes by tuning the interface-hopping amplitude or by selecting a CI of appropriate band effective mass. More importantly, we find that a topologically trivial TI slab can be made non-trivial and vice-versa by tuning of such an interface-hopping amplitude or by tuning the CI band effective-mass; namely, a topological phase transition can be induced in such heterostructures indicated by the presence or absence of gapless linear edge modes. We discuss the relevance and realization of our results and conclusions in future experiments.

Keywords: topological insulator, interface of topological insulators, edge states, topological surface states

(Some figures may appear in colour only in the online journal)

1. Introduction

The three-dimensional topological insulator (TI) Bi_2Se_3 and other members of the same crystallographic family are extensively studied systems since Zhang *et al* [1] predicted and Hasan *et al* [2] verified experimentally their topological nature. Due to their symmetry protected robust electronic dispersion and other features, such as absence of backscattering, TIs are considered to be useful in quantum information and computing. However, the integration of TIs in electronic devices seem far from realization due to many practical problems, including the small surface to bulk ratio of the topological conduction channels, and the interference of bulk conduction states to the surface phenomena due to the small band gap.

By virtue of the bulk-boundary correspondence, the topological surface states of the TIs can also be localized at the interface between the topological and a topologically trivial material, such as, a conventional insulator. Occurrence of topological states at the interfaces between a TI and different types of topologically trivial materials have been long predicted and established experimentally [3–6]. This is a very important property of the TI as the interface allows more control and manipulation of the topological states. Moreover, interfaces can give rise to qualitatively different phenomena compared to the bulk [7, 8].

Utilization of interfaces, such as the PN junction, is a common approach in almost all modern day electronic devices. Future electronic applications, in which the TI plays a role, may also utilize interfaces. The 'interface' of the TI with vacuum, i.e. the TI surface, has been thoroughly studied and rather well understood [9]. There have been many efforts recently to understand the phenomena at the interface of a TI with different materials, e.g. metals, conventional insulators [10, 11], as well as other materials [4, 12, 13]. It has also been demonstrated experimentally that the surface bands of

the TI can be modulated by modifications of the surface [5]. However, very few systematic studies [14, 15] have been performed on ultra-thin TIs interfaced with topologically trivial insulators.

Recently, a few studies have been directed to understand and use thin TI materials in device application as the surface to bulk ratio is comparable. However, the wave-functions of the Dirac-like topological states that appear on the opposite surfaces and interfaces of a three-dimensional TI have a finite width. This leads to overlap and hybridization between the top and bottom Dirac surface states when the thickness of the TI slab becomes comparable to the wave-function width and this opens up a gap [16, 17] in the Dirac spectrum. The band-gap as a function of thickness of the slab has been well studied in previous investigations [18] which show that 5 quintuple layers (QLs) is the critical thickness of a Bi_2Se_3 slab necessary for obtaining a Dirac-like linear dispersion with a negligible gap ($\sim$10 meV gap). Several methods have been proposed, such as, applying electric field in thin films [19] or designing interfaces with different materials [20, 21], in order to overcome the quantum limit so that ultra thin TIs can still host topological surface states. It has been predicted [22, 23] and experimentally verified [24] that the band-gap formed this way at the Dirac point (DP) of the surfaces of a pure thin TI slab behaves non-monotonically as a function of slab thickness. Several theoretical studies on pure thin TI films suggest that the system oscillates from a quantum-spin hall (QSH) phase that hosts non-trivial edge modes to a trivial insulator phase [25–27]; however, such QSH modes have not been observed experimentally yet, mainly because the band-gap of the bulk states is too small to resolve the presence of edge modes.

In the present work, we study the interface between a thin topological insulator (TI) and a conventional insulator (CI) in a 'sandwich' geometry. We use the model Hamiltonian of Zhang *et al* [1] which, because of its simplicity and completeness, allows us to understand the problem deeper and to study the phenomena by varying the various parameters, such as, the interlayer hopping amplitude, band-gap, ionization potential and effective mass. Our calculations for the interface geometry of the TI-CI heterostructure suggest that the band gap of the interface Dirac cone can be tuned by varying the coupling strength of the hybridization between the electronic states of the two materials or the CI band effective-mass. More importantly, a topological phase transition can be induced in such heterostructures for any thickness of the TI material. Such topological phase transition is indicated by closing and opening of the band-gap, at the interface Dirac point, which is the hallmark of the topological phase transition in non-interacting systems. Recently, a topological phase transition as a function of the TI length and the ionization potential was reported [15] in the interface geometry using a different approach, the so-called envelope-function approximation. We also demonstrate in detail the emergence of the edge modes in a ribbon geometry in the case of the appearance of non-trivial topology. Last, we study the conditions upon which such non-trivial edge states can be detected by angular resolved photoemission spectroscopy (ARPES).

The remainder of the paper is organized as follows. In section 2, we describe our formulation and computational details used in this work. In section 3, we present our main results from interface model Hamiltonian calculations. Finally, in section 4, we present our conclusion and implications for further studies.

2. Model and formulation

In order to study the interface of TI with CI, we started from the well-known 4×4 model Hamiltonian of Zhang *et al* [28] for the TI material which is given by:

$$\begin{aligned}\mathbf{H}_{\mathrm{TI}}(\vec{k}) = (-M_0 + M_1 k_z^2 + M_2 k_\perp^2)\Gamma_5 \\ + B_0\Gamma_4 k_z + A_0(\Gamma_1 k_y - \Gamma_2 k_x),\end{aligned} \tag{1}$$

where Γ are the well-known Dirac matrices. The parameters M_0, M_1, M_2, B_0, and A_0 in the Hamiltonian are taken to be positive. The negative sign in front of the M_0 term makes the Hamiltonian inverted which guarantees the presence of the topological surface states. When the thickness of the TI is made smaller, it opens up a gap in the topological surface state due to the hybridization of the states from the opposite surfaces. Such effect is captured by this model Hamiltonian when the thickness becomes smaller than 30 Å.

We are interested in thin layers of TI when it is interfaced with a CI using an atomistic tight-binding approach. For this, we will define a four Wannier-orbital tight-binding Hamiltonian (i.e. a lattice of four atomic orbitals per unit cell) with hopping matrix elements such that when this Hamiltonian is transformed into k-space, it reproduces the same 4×4 model Hamiltonian of Zhang *et al* [28] in the limit of small k, i.e. in the vicinity of the Γ point. Namely, the lattice version of this Hamiltonian describes a fictitious TI system which gives the same band structure as the Bi_2Se_3 Hamiltonian. The unit cell of such fictitious TI system contains two states described by spin hopping between states of opposite parity within the unit cell and nearest neighbor hopping between states of same spin.

For simplicity, the conventional non-topological insulator part of our interface is modeled by taking similar 4×4 form of the Hamiltonian as that of the TI but without the band inversion term i.e.

$$\begin{aligned}\mathbf{H}_{\mathrm{CI}}(\vec{k}) = (M_0' + M_1' k_z^2 + M_2' k_\perp^2)\Gamma_5 \\ + B_0'\Gamma_4 k_z + C_0 I,\end{aligned} \tag{2}$$

where C_0 is the band energy offset (also called as ionization potential (IP)) between the TI and the CI and M_0', M_1', M_2', and B_0' are the parameters of the CI which depend on the energy band properties of the specific CI material. The role of C_0 is to shift the overall bands. In the interface calculations, the C_0 term shifts the DP away from zero. The CI described by the Hamiltonian of equation (2) has a band-gap of $2M_0'$. In figures 1(b) and (c), we show the energy dispersion of the TI and CI Hamiltonian given in equations (1) and (2) for open boundary conditions along one direction ($\hat{z}$-direction) and periodic boundary conditions along the other two

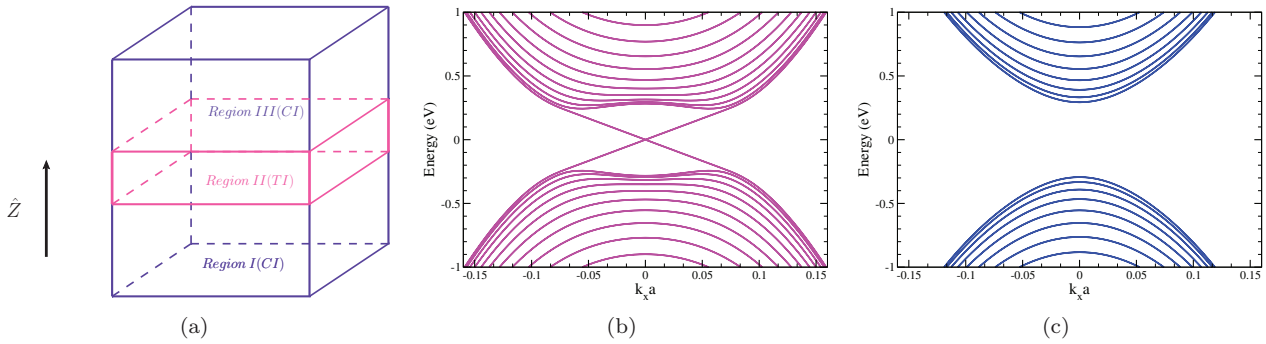

Figure 1. (a) The geometry of the CI-TI-CI interface used in our calculation where TI is sandwiched in between CI (red block). (b) and (c) Slab band structure obtained by diagonalizing the TI and the CI Hamiltonian given in equations (1) and (2) respectively.

perpendicular directions. Setting $B_0' = 0$, which is the coupling between bands of different parity will not change the following conclusions.

We study the three-layer heterostructure shown in figure 1(a) containing CI-TI-CI, where a thin layer of TI is sandwiched between two symmetric insulators. For this, we divide the system into three regions. Region I and III lie from lattice sites $-\infty$ to $-(n+1)$ and $(n+1)$ to ∞ respectively and are described by the CI Hamiltonian whereas region II extends from $-n$ to n sites and is described by the TI Hamiltonian. In region II, the Hamiltonian is written as:

$$\mathbf{H}_{\mathrm{II}}(k_x,k_y) = \sum_{\alpha,\beta}\Big[\sum_i V_{\alpha\beta}|i,\alpha\rangle\langle i+1,\beta| + \mathrm{h.c.}\Big] + \sum_{\alpha,\beta,i} E_{\alpha\beta}|i,\alpha\rangle\langle i,\beta| \tag{3}$$

where the index i denotes lattice sites, i.e. unit cells which contain four Wannier orbitals denoted as $|i,\alpha\rangle$. Here, α and β indices denote (μ,σ) and $\mu = \pm 1$ stands for the positive and negative parity states and σ stands for the spin. Similarly the Hamiltonian for region I and III in discretized form is written as:

$$\mathbf{H}_{\mathrm{I/III}}(k_x,k_y) = \sum_{\alpha,\beta}\Big[\sum_i V'_{\alpha\beta}|i,\alpha\rangle\langle i+1,\beta| + \mathrm{h.c.}\Big] + \sum_{\alpha,\beta,i} E'_{\alpha\beta}|i,\alpha\rangle\langle i,\beta|. \tag{4}$$

The $\mathbf{V}$ and $\mathbf{V}'$ are the interface-hopping matrices within the TI and CI atomic orbital sites respectively and $\mathbf{E}$ and $\mathbf{E}'$ are the corresponding 'on-site' matrices. Their specific form can be derived easily from the discretization of the Hamiltonian in the respective regions by performing the standard $k_z \to -i\frac{\partial}{\partial z}$ transformation which is written below for completeness:

$$\mathbf{E} = \big[-M_0 + \frac{2M_1}{a^2} + M_2 k_\perp^2\big]\Gamma_5 + A_0(\Gamma_1 k_y - \Gamma_2 k_x), \tag{5}$$

$$\mathbf{E}' = \big[-M_0' + \frac{2M_1'}{a^2} + M_2' k_\perp^2\big]\Gamma_5 + C_0 I, \tag{6}$$

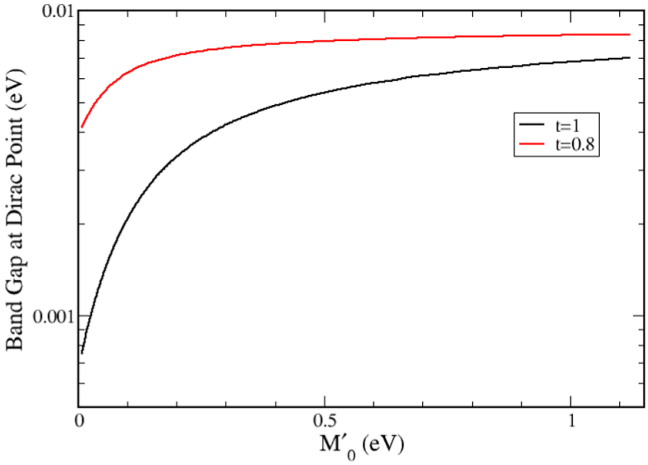

Figure 2. The dependence of the TI interface state band-gap on the gap M_0' of the CI.

$$\mathbf{V} = -\frac{M_1}{a^2}\Gamma_5 - i\frac{B_0}{2a}\Gamma_4, \tag{7}$$

$$\mathbf{V}' = -\frac{M_1'}{a^2}\Gamma_5 - i\frac{B_0'}{2a}\Gamma_4, \tag{8}$$

where a is the lattice spacing used for the discretization of the differential operator and is unrelated to the length scales which characterize the crystalline unit cell or atomic distances.

At the boundary between the TI and the CI, we couple orbitals of the TI system at the $\pm n^{\mathrm{th}}$ layer with CI orbital at the $\pm(n+1)^{\mathrm{th}}$ layer by the following Hamiltonian:

$$\mathbf{H}_{\mathrm{b}} = T_{\alpha\beta}\Big[|n,\alpha\rangle\langle n+1,\beta| + |-(n+1),\alpha\rangle\langle -n,\beta|\Big] + \mathrm{h.c.}. \tag{9}$$

where $\mathbf{T}$ is the coupling matrix and it depends on the microscopic details of the interface. We consider the simplest form of the coupling matrix term that connects the same states between TI and CI which is given by:

$$\mathbf{T} = t(-\frac{M_1}{a^2}\Gamma_5 - i\frac{B_0}{2a}\Gamma_4), t \geqslant 0. \tag{10}$$

This form of the interface-hopping matrix is motivated by the hopping inside the TI as seen in equation (8). When $t = 1$ and

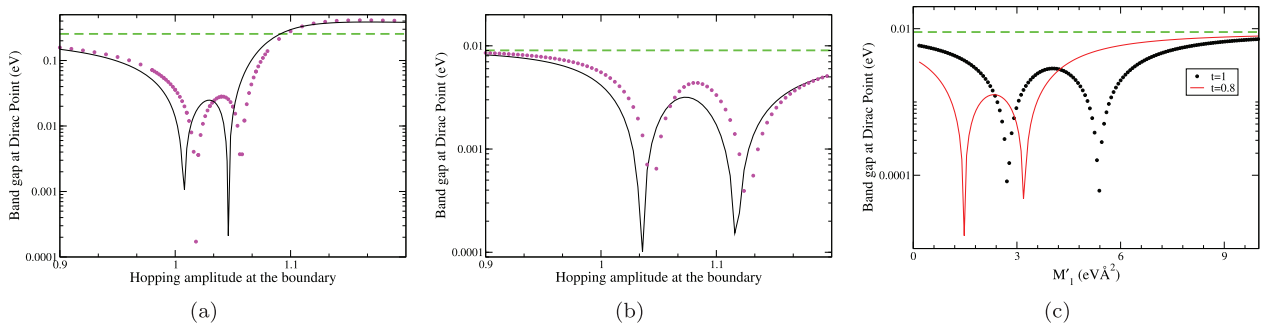

Figure 3. Band gap at the DP for the interface Hamiltonian defined in section 2 for TI thickness of $L = 15.55$ Å (a) and $L = 31.1$ Å (b) as a function of the interface-hopping parameter t. Notice that the band-gap closes at two values of t, say t_{c1} and t_{c2}. Panel (c) gives the dependence of the interface Dirac-state band-gap on the band-curvature M_1' of the CI. In sub-figures (a) and (b) the band-gap of the CI (M_0') considered are 0.28 eV for the black solid line and 0.56 eV for dotted magenta dots in both curves. The dashed horizontal green line in all the sub-figures indicates the value of band-gap for $t = 0$ at the interface which is equivalent to an infinite wall at the boundary. Notice that, unlike the anticrossing as a function of length in pure TI slab, dips are actually band crossing points.

$H_{\rm CI}$ is replaced by $H_{\rm TI}$, this situation corresponds exactly to a thick TI slab facing infinite potential wall at the boundary of the heterostructure whereas $t = 0$ case corresponds to the situation where TI and CI are completely decoupled and are separated by the infinite wall. For simplicity, we consider the interface-hopping between different parity states (i.e. the second term in equation (10)) from the TI to the CI and vice-versa to be zero in all the calculations presented in this work as it does not affect our conclusions.

For the nano-ribbon geometry, the Hamiltonian is discretized along both $\hat{z}$ and $\hat{x}$ direction whereas $\hat{y}$ is considered as the translationally invariant direction. The lattice parameters along $\hat{x}$ and $\hat{z}$ direction were taken to be ∼7–15 Å and ∼1–3 Å respectively as the decay length of the wavefunction along $\hat{x}$ is very long compared to $\hat{z}$ direction. Similarly, the number of lattice points along $\hat{x}$ and $\hat{z}$ directions are taken to be ∼100–200 and ∼50–100 respectively.

We also investigated the interface geometry discussed here formed from very thick layers of TI and CI. In this case we can idealize the system as a CI-TI-CI system where each of the layers is thick enough to assume that it is governed by the pure bulk Hamiltonians. If the TI layer is very thick, the Hamiltonian of Zhang *et al* [28] which is only valid in the long-wavelength limit (small k limit near the Γ point) is applicable. In this case we assume that the three layers are ideal layers governed by the ideal bulk Hamiltonians. Therefore, we need to find the boundary condition for the wavefunction at the interface in the usual fashion, namely by integrating the Schrödinger equation along an infinitesimal region which encloses the interface. We describe this approach in the appendix along with our conclusions. Our main conclusion is that the main result found with our approach discussed in the main manuscript that there is a topological phase transition in thin TI interfaced with CI is valid even for this different BC.

3. Results

In this section we study the effect on the band-gap of the topological interface state played by the interface-hopping term and the parameters which define the CI Hamiltonian. We find that, as a function of the strength of t that defines the coupling between the TI and CI or the effective mass of the CI bands, there exists a topological phase transition. Next, in section 3.1 we discuss the topological phase transitions that we found. In section 3.2 we discuss the influence of the above mentioned parameters on the band structure of the interface states and their corresponding wavefunctions. In section 3.3 we explore the appearance of QSH edge states for nano-ribbon geometries. Finally, in section 3.4 we give an interpretation of our results.

3.1. Topological phase transitions

In figure 2 we illustrate the dependence of the gap at the interface Dirac cone as a function of the CI bulk band-gap M_0'. Notice that it is an increasing function of M_0' and for large values of M_0' it reaches the gap value of the surface Dirac state of an isolated TI of the same thickness, as expected.

In figure 3, we present the gap observed at the surface DP as a function of the interface-hopping strength t for different values of thickness of the TI using different sets of band-gap and band-curvature parameters of the CI. We find that the gap E_G at the DP of the surface Dirac states even for a very thin TI, for which E_G is of the order of 100s meV due to the hybridization between the top and bottom surface states, can be closed by interfacing it with a CI for some value of the interface-hopping strength between the TI and CI. For example, in figure 3(a), we see that even though the band-gap of a thin TI at the DP is as big as 0.25 eV for infinite potential wall, such a gap can decrease and ultimately become zero for t close to 1. In fact, we find that the band-gap vanishes at two values of t (t_{c_1} and t_{c_2}) forming a 'dome-like' shape close to $t = 1$. Such 'dome' is observed for a wide range of band-gaps of the CI and for different thickness of the TI. Even a thick TI, which has negligible gap (of the order of μeV), has similar 'dome' shaped behavior. Moreover, such closing and reopening of the band-gap is an indication of topological phase transition. More will be discussed regarding this topological phase transition in section 3.2.

Previous studies have seen oscillatory gap closing in pure TI and heterostructures as a function of length and the

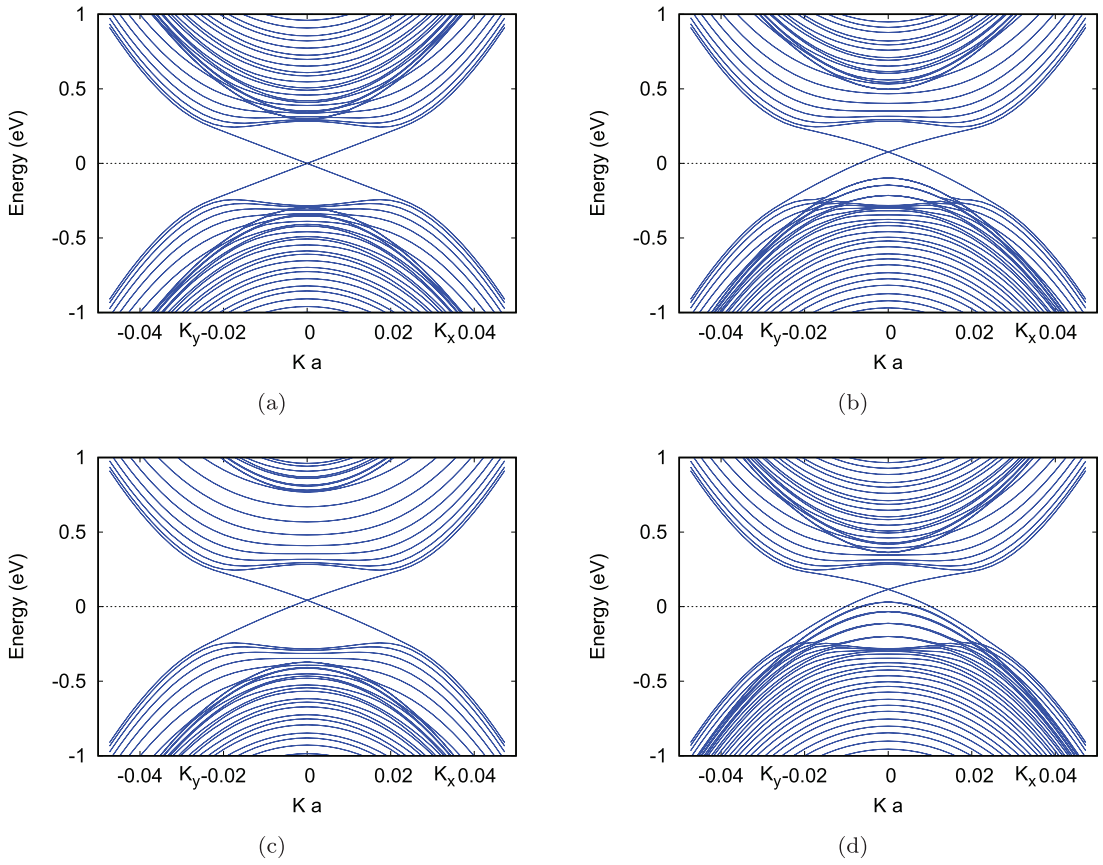

Figure 4. Interface bands for different values of IP (C_0) and band-gap of the CI (M_0'). The values of C_0 and M_0' taken are (a) $C_0 = 0\,\text{eV}$, $M_0' = M_0$ (b) $C_0 = 0.2\,\text{eV}$, $M_0' = M_0$ (c) $C_0 = 0.2\,\text{eV}$, $M_0' = 2M_0$ and (d) $C_0 = 0.2\,\text{eV}$, $M_0' = 0.5M_0$. Notice the shift of the CI bands and the shift of the DP. The shift of DP is ∼75 meV, ∼40 meV and ∼110 meV in (b), (c) and (d) respectively.

ionization potential of the TI [15]. Oscillatory evolution of the band-gap at the surface DP as a function of the TI thickness is also visible in our heterostructure geometry. Such oscillation can also be observed for a fixed thickness of the TI slab as a function of the M_1, where M_1 is the band curvature of the TI. This is because our varying of length amounts to varying the interface-hopping parameters in the Hamiltonian. However, the gap closing and opening as a function of the hopping strength seen in figure 3 has not been reported before in the literature. The 'dome-shaped' form can also be obtained for a fixed t in the heterostructure geometry as a function of the band curvature of the insulator (M_1') as illustrated in figure 3(c). This implies that tuning the hopping strength at the interface is physically similar to tuning the band curvature of the insulator in contact and could provide one more way of engineering the topological phase transition in the interface.

The role of the ionization potential or band offset term C_0 is to shift the overall bands of the insulator as illustrated in figure 4. Because of such shift, the DP moves away from zero depending on the sign of C_0. Also, the linearity regime of the Dirac states decreases.

We note that the model Hamiltonian we are using is a bulk Hamiltonian and the results of the Hamiltonian are only valid as the thickness of the TI approaches the bulk limit for open boundary condition (slab geometry). Having said this, it is also remarkable that the model Hamiltonian is able to capture the topological features of a thin slab containing just few QLs as has been demonstrated in [22]. Hence, we believe that our conclusions of the topological phase transitions are valid in thin limit of the TI (of a few QLs) as long as the TI model Hamiltonian is valid.

3.2. Band-structure and wavefunction of the interface Hamiltonian

In this section, we examine the band structure and wavefunction of our heterostructure at different values of the interface-hopping parameter t by keeping the thickness of the TI constant. This will help us elucidate the nature of the bands and the localization of the wavefunction when the band-gap changes. Moreover, as illustrated in figure 3 we found that, as a function of the interface-hopping strength, the band-gap of the interface states closes and reopens. Such closing and reopening of the band-gap is an indication of a topological phase transition and deserves further investigation.

In figure 5, we show the interface band structure along the k_y direction. The gray background shows the states of a thick TI slab whereas the red lines show the bands for the heterostructure. Similarly, in figure 6, we show the corresponding wavefunctions of the valence state closest to the zero energy at the Γ point as a function of distance along the $\hat{z}$ direction. The wavefunction at each $k_x - k_y$ point is a four component spinor with projections on the 4 basis states $|P1_z^+, \uparrow\rangle$, $|P2_z^-, \uparrow\rangle$, $|P1_z^+, \downarrow\rangle$, and $|P2_z^-, \downarrow\rangle$, where the $+$ or $-$ superscript stands for

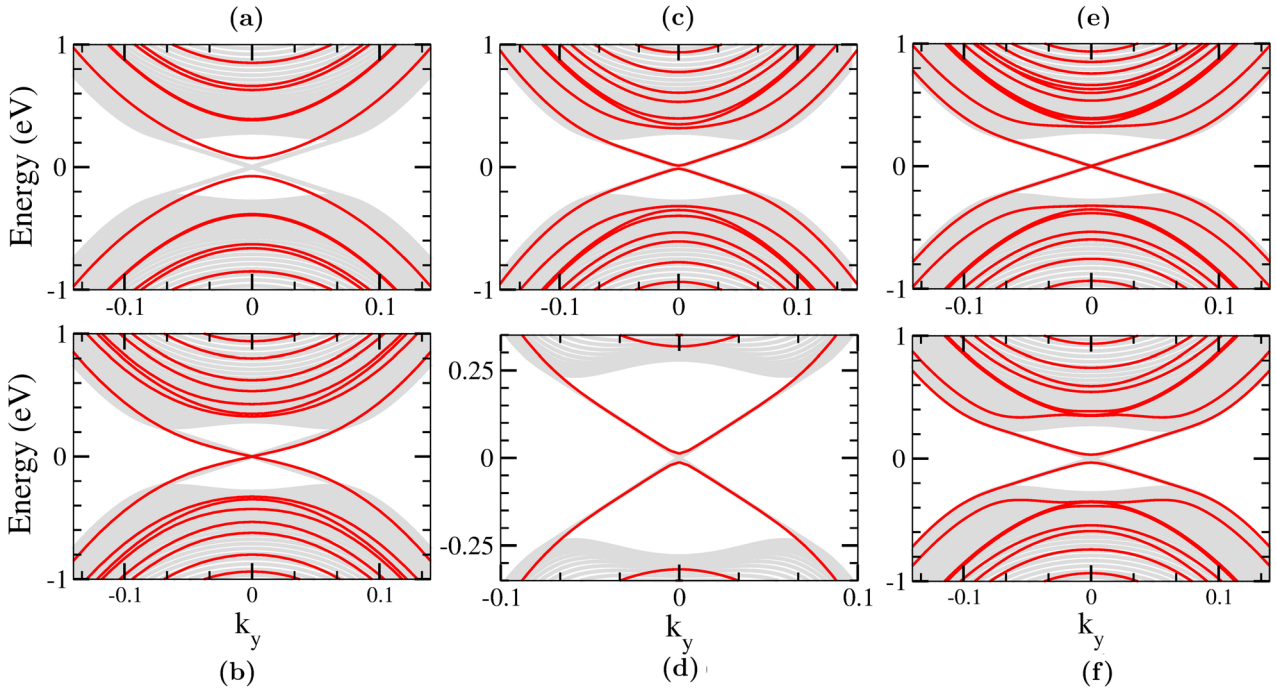

Figure 5. Band structure along the k_y direction at different values of the interface hopping parameter t shown in figure 3(a) for CI band-gap (M_0') of 0.28 eV. The value of the interface hopping strength t are taken to be (a) 0.9 (which is less than t_{c1}), (b) 1.008 (which is at t_{c1}), (c) 1.015 (in between t_{c1} and t_{c2}), (e) 1.046 (which is at t_{c2}) and (f) 1.06 (which is slightly above t_{c2}). Figure (d) is zoomed version of figure (c). See text for details.

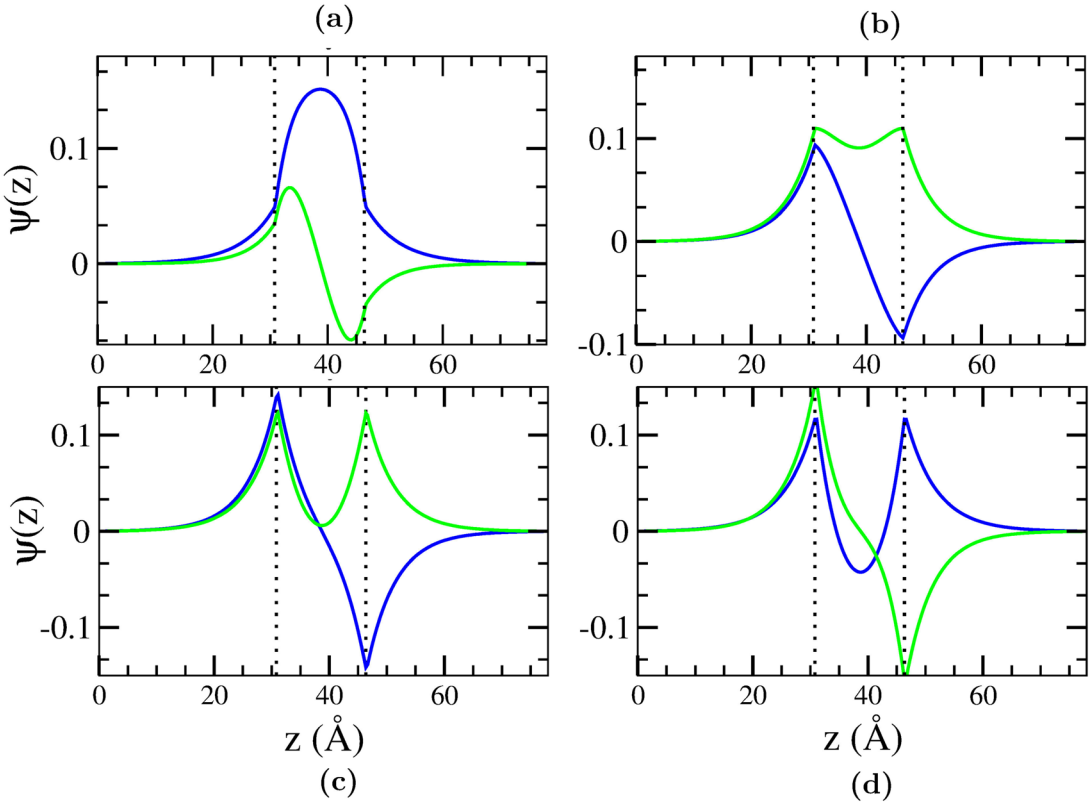

Figure 6. Wavefunctions at the Γ point for one of the eigenstates corresponding to the lower Dirac branch shown in figure 5 as a function of distance along the $\hat{z}$-direction. The value of t are (a) 0.9 (less than t_{c1}), (b) 1.01 (slightly beyond t_{c1}), (c) 1.04 (slightly less than t_{c2}) and (d) 1.06 (beyond t_{c2}). The green curves denote positive parity states whereas the blue curves denote negative parity states. See text for details.

the two bonding or antibonding combinations formed from the two atomic p_z orbitals of a pair of Bi ($P1$) and and a pair of Se atoms ($P2$) in the unit cell. These 4 states form the conduction and valence bands of the topological insulator. In addition, $\pm$ corresponds to the parity of the states and $\uparrow$ and $\downarrow$ stand for the two spin projections. At the Γ point, the Hamiltonian is diagonal in spin space and, hence, the wavefunction has only two components of opposite parity but of the same spin. In figure 6, the green and blue lines denote states of positive and negative parity respectively. We see that the positive and negative parity states change their spatial symmetry at different points in the range of the interface-hopping parameter t.

In figure 3, we saw that there are two values of hopping strength where the gap closing occurs. When we look at the band structure and the wavefunction at each of these critical points, we find different behavior. The wavefunction at the first gap closing point (t_{c1}) has significant overlap with the bulk. On the other hand, the wavefunction at the second gap closing (t_{c2}) is similar to the surface states of the pure TI slab where the bulk atoms have negligible contributions. The close connection of the second gap closing point with the surface states of the pure TI slab can also be inferred from the fact that the bands below the Dirac like states are in an inverted regime (See figures 6(b) and (c)).

Note that if, instead of the CI-TI-CI interface, we consider a TI-CI interface where the TI is in contact with the CI on only one side and on the other side the TI faces an infinite potential well, then we do not find a 'dome' shaped form of the band-gap as a function of the interface-hopping strength. Namely, the gap at the interface DP closes at just one value of the interface hopping which happens to be in between the two gap closing points for the sandwich geometry.

3.3. Exploration of the quantum Spin-Hall states

The interface geometry preserves inversion symmetry similar to the TI bulk. Hence, we can use the prescription of Fu and Kane [29] to find out whether the system hosts topological edge states by calculating the parity of the wavefunctions. The overall parity of the wavefunction is determined by the parity of both the spatial part of the wavefunction $f(z)$ and and the parity of the basis set. In figure 6(a), we see that $f(z)$ is symmetric for the negative parity components of the wavefunction and anti-symmetric for the positive parity components. Hence, the total parity of the valence state wavefunction is negative. However, for the same state after the first band crossing point in figure 6(b), we find that $f(z)$ is anti-symmetric for the negative-parity components of the wavefunction and symmetric for the positive-parity components making the overall parity of that state positive. Following Fu and Kane's construction, in order to make a statement about the non-trivial topology for our heterostructure, we should find the product of the parity of all the valence bands. Hence, our above conclusion does not guarantee the presence of non-trivial topology. Nevertheless, such switching of parity signals the existence of such state. Moreover, we know that a thin TI is topologically trivial which is the case of our heterostructure in the $t \to 0$ limit. As the value of t increases beyond the first band crossing, t_{c1} , the topology changes, i.e. a trivial system becomes topological and vice-versa.

In order to verify the presence or absence of non-trivial topology, we consider a nano-ribbon of heterostructure which is finite in the $\hat{x}$ and $\hat{z}$ direction but infinite in the $\hat{y}$ direction. In figure 7, we show the nano-ribbon bands and the corresponding wavefunctions for our heterostructure consisting of TI of thickness $L_z = 18$ Å and width $L_x = 1600$ Å sandwiched between CI material of same thickness and width. As seen in figure 7(a), the system is trivial before t_{c_1} indicated by the absence of any zero energy states. However, after t_{c_1}, the system is in a QSH phase as seen by the presence of Dirac-like states in figure 7(b). In addition, the wavefunctions corresponding to the Dirac-like states at the Γ point in figures 7(a) and (d) show the presence of the localized edge modes.

The possibility of existence of the QSH phase even for a thin TI material in a heterostructure geometry, provided that the model Hamiltonian is still valid in small thickness limit, is indeed very exciting and could have many potential applications. It is well known that for the case of pure TI slab, there is a cutoff thickness below which the system is topologically trivial, e.g. for TI Bi_2Se_3, the minimum thickness necessary for the system to be in QSH phase is 27 Å. However, we found that, by making an interface between a TI with a CI, even a thin TI, which is in a trivial phase, can be tuned to a QSH phase for some value of the hybridization strength t. Similarly, a TI in QSH phase can be made trivial. Hence, it seems possible to use the coupling strength t (which is equivalent to the tunneling of the electrons to and from the TI and CI), as a knob to switch the topological character of the heterostructure.

3.4. Interpretation and discussion of our results

In order to understand the reason for the band closing and reopening as a function of the coupling strength at the interface, we consider a simple 4×4 Hamiltonian to describe the edge states due to the coupling between the TI and the CI states for an asymmetric interface where TI is interfaced with CI on only one side.

In the basis of the $|T+\rangle, |T-\rangle, |C+\rangle, |C-\rangle$, where, T(C) denotes TI(CI) states, we can write the following coupling matrix at $k_x = k_y = 0$ neglecting the spin:

$$\mathbf{H}(k_z, k_z') = \begin{bmatrix} T(k_z) & -\mathrm{i}B_0 k_z & -\gamma & 0 \\ \mathrm{i}B_0 k_z & -T(k_z) & 0 & -\gamma \\ -\gamma & 0 & C(k_z') & -\mathrm{i}B_0' k_z' \\ 0 & -\gamma & \mathrm{i}B_0' k_z' & -C(k_z') \end{bmatrix}, \quad (11)$$

where, $T(k_z)$ and $C(k_z')$ denote the TI and the CI states respectively and are given by:

$$T(k_z) = -M_0 + M_1 k_z^2, \quad (12)$$

$$C(k_z') = M_0' + M_1' k_z'^2. \quad (13)$$

γ is the coupling matrix element between the TI and the CI states of the same parity. Similarly, B_0 and B_0' are the coupling

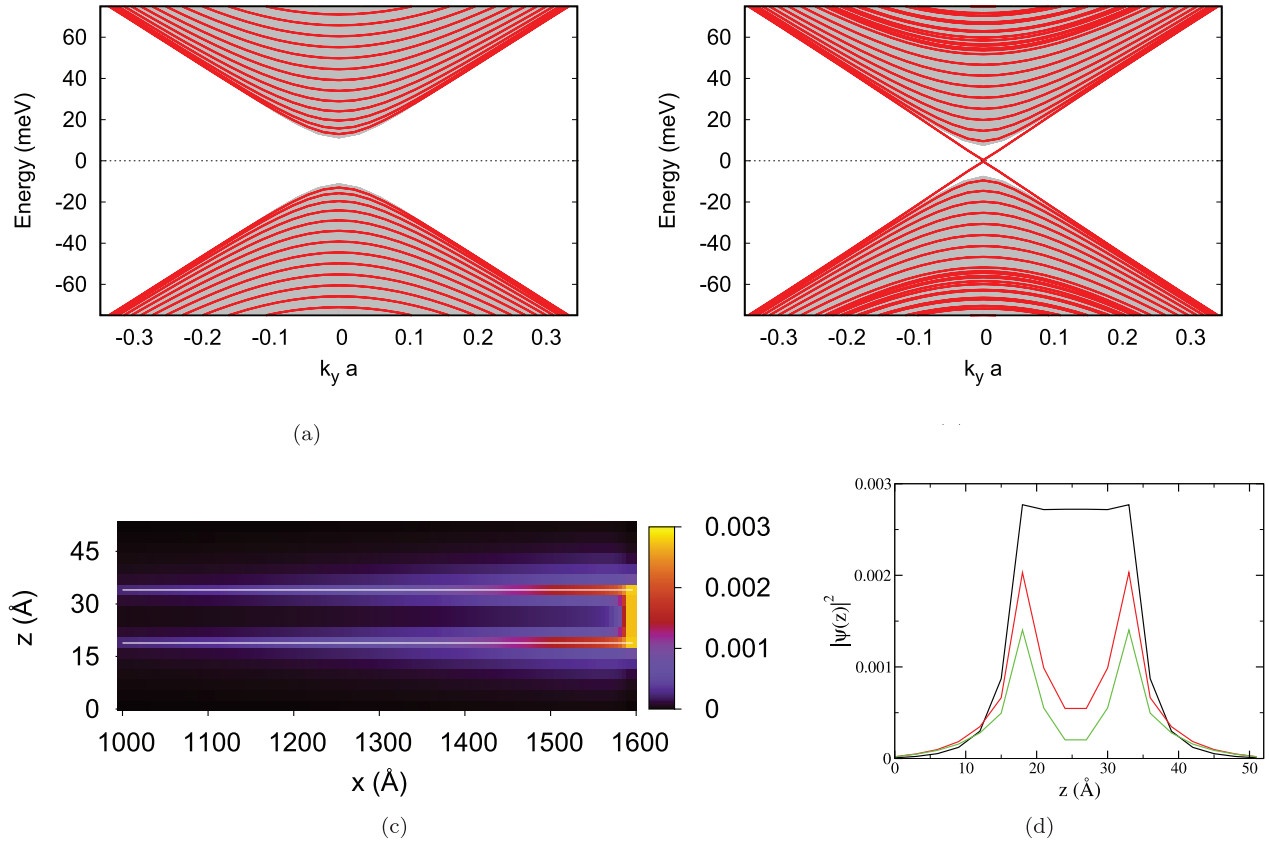

Figure 7. Band structure and wavefunction of the interface bands for the nano-ribbon geometry. In subfigures (a) and (b), we show the nano-ribbon band structure (the red lines) for $t < t_{c1}$ and $t > t_{c_1}$ respectively. The gray background denotes the bulk states of the nano-ribbon. Notice that in (a), there are no edge states whereas in (b), there are Dirac like states lying in the bulk gap. In subfigure (c), we plot the square of the wavefunction of the Dirac-like state at one edge of the heterostructure which shows peaks on the two edges. There are similar states at the other edge of the nano-ribbon. The white horizontal line denotes the boundary between the TI and CI. In subfigure (d), we show the z-dependence of the edge state wavefunction at different values of x. The black line is for a value of x close to the edge of the box and red (green) line is 5 (20) lattice-spacings away from the edge.

matrix element between the opposite parity states within the TI and the CI respectively.

Since we only couple states at the interface in our full diagonalization problem, it seems reasonable to couple states of the TI and the CI that are only localized at the interface in our effective interface Hamiltonian (equation (11)). From the TI side, the state closest to the zero energy, which has Dirac-like dispersion, is localized at the interface. Other higher energy states from the TI are delocalized and have bulk-like properties. Hence, we only consider few states from the TI that is closest to the zero energy state. Similarly, we consider the lowest eigenstate of the CI as our results are valid even for a thin CI case.

When B_0 and B_0' are set to zero, we have quantized energy levels similar to the particle in a box problem given by:

$$k_z = \frac{n\pi}{L_{\rm TI}}, k_z' = \frac{n'\pi}{L_{\rm CI}}, \tag{14}$$

$$T(n)_{\pm} = \pm(-M_0 + M_1(\frac{n\pi}{L_{\rm TI}})^2), \tag{15}$$

$$C(n')_{\pm} = \pm(M_0' + M_1'(\frac{n'\pi}{L_{\rm CI}})^2), \tag{16}$$

where n and n' are independent positive integers and $L_{\rm TI(CI)}$ is the length of the TI(CI) considered. Equation (11) is block diagonal when $B_0 = B_0' = 0$. The eigenvalues are:

$$E_1^{\pm} = \frac{T(k_z) + C(k_z')}{2} \pm X, \tag{17}$$

$$E_2^{\pm} = \frac{-T(k_z) - C(k_z')}{2} \pm X, \tag{18}$$

$$X = \sqrt{\left((T(k_z) - C(k_z'))/2\right)^2 + \gamma^2}. \tag{19}$$

In figure 8(a), we plot the energy levels given by equations (17) and (18) as a function of the coupling strength γ by coupling $n = 1$ and $n = 2$ levels of the TI with the lowest level (i.e. $n' = 1$) of the CI when the material parameters (M_0, M_1) are considered to be the same for the TI and the CI. A value of $L_{\rm TI} = 20$ Å and of $L_{\rm CI} = 50$ Å (similar to those used in figure 3) were used. For comparison, we also show the eigenvalues as a function of the coupling strength from the full diagonalization problem for the asymmetric interface in figure 8(b) with and without the B_0 term. The similarity of the

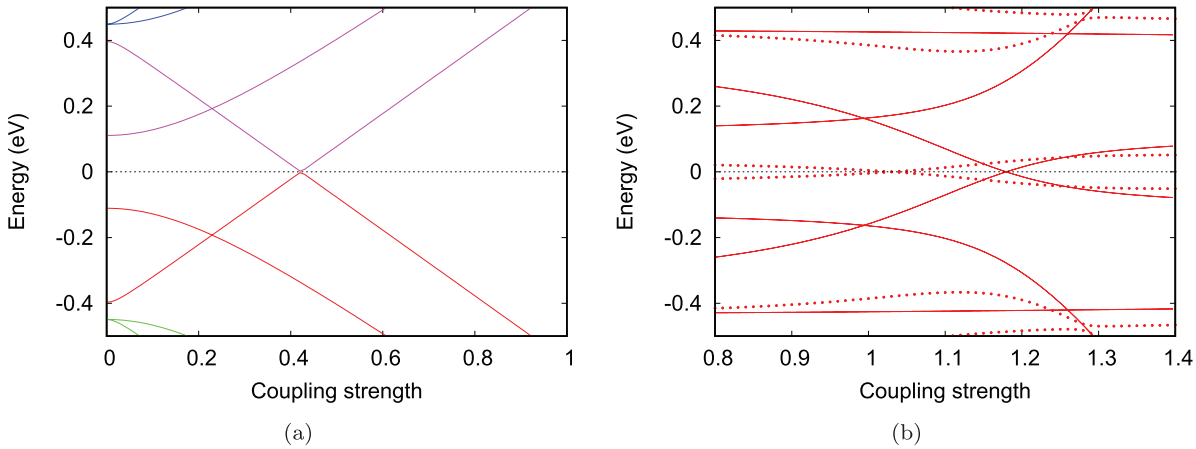

Figure 8. Evolution of the eigenvalues at the Γ point as a function of (a) γ obtained from equation (19) and (b) t from the full diagonalization of the asymmetric interface problem. In figure (b), the solid lines (red dots) are the eigenvalues when B_0 term is turned off (on).

energy scale and the crossing of the levels even above the zero energy shows that the assumptions we made about the coupling of lowest lying levels between the TI and CI are valid in the vicinity of the Fermi level. Moreover, we see from figure 8(b) that the role of the B_0 term is to shift the zero energy crossing and gap out the crossings between the higher states. We note that from our effective interface Hamiltonian, we can obtain level crossing as a function of γ by coupling only the $n = 1$ level of TI with $n' = 1$ of the CI when $T(n = 1) > 0$. This happens when $L_{\rm TI} < \pi\sqrt{\frac{M_1}{M_0}}$ and corresponds to a TI other than Bi_2Se_3 for which the parameters of this Hamiltonian are obtained [28].

4. Conclusion and outlook

We studied the interface of the topological insulator Bi_2Se_3 with a conventional insulator using the model Hamiltonian that describes this TI. Our model interface calculations suggest that it is possible to tune the gap induced in the surface Dirac cone of a thin layered topological insulator by designing heterostructures with a conventional insulator. Moreover, we found that a topological phase transition can be induced in such heterostructures where we can switch back and forth the character of the interface from a quantum-spin hall phase to a topologically trivial phase, as a function of the coupling strength between the topological and conventional insulator. Such a topological phase transition can be also achieved by tuning the band curvature of the conventional insulator in contact. Experimentally, it might be possible to tune the coupling strength between the topological and conventional insulator by application of pressure.

We found that the critical values of the interface hopping and the CI band mass are within the range of physically realizable values in real materials. For example the critical values of the ratio of the interface hopping to the electron hopping matrix element inside the TI is of order unity. Furthermore, the critical value of the CI band effective mass is also of order of the bare electron mass as shown in figure 3(c). Therefore, this prediction can be verified experimentally where the precise value of the interface hopping parameter t depends on many factors which cannot be easily captured by DFT calculations. However, for any given reasonable value of t, one can experimentally choose a CI with an appropriate band-gap and band effective-mass which correspond to either topologically non-trivial or a trivial interface. In the topologically non-trivial interface, edge states would be observed in a nano-ribbon geometry as illustrated in the present work.

Direct experimental observation of quantum spin-hall states in thin TI films has so far been unsuccessful due to the small gap (a few meV) which opens at the surface Dirac cone for a wide enough TI slab to be in the topological phase. In the present work we found that a thin TI, which would be in the topologically trivial phase, can be made topological by interfacing it with an appropriate CI. The band gap for such topological interface Dirac state turns out to be more than a factor of two bigger than the maximum gap of the pure TI in the topological phase (See figure 3). Such two-fold increase in the band-gap of the Dirac interface state is within the resolution range of the ARPES technique [20, 21, 24] and, thus, such an interface may allow a direct experimental observation of the edge states in the near future.

Since interfaces are very important for designing next generation electronic devices, we believe that our work will guide future works towards systematic designing and understanding of the topological character of such interfaces.

Acknowledgments

This work was supported in part by the U.S. National High Magnetic Field Laboratory, which is funded by NSF DMR-1644779 and the State of Florida.

Appendix. Boundary condition in the thick layer limit

Here we discuss our implementation of the boundary condition [30] which is more appropriate for an interface formed by very thick layers of TI and CI. In this case we can idealize the system

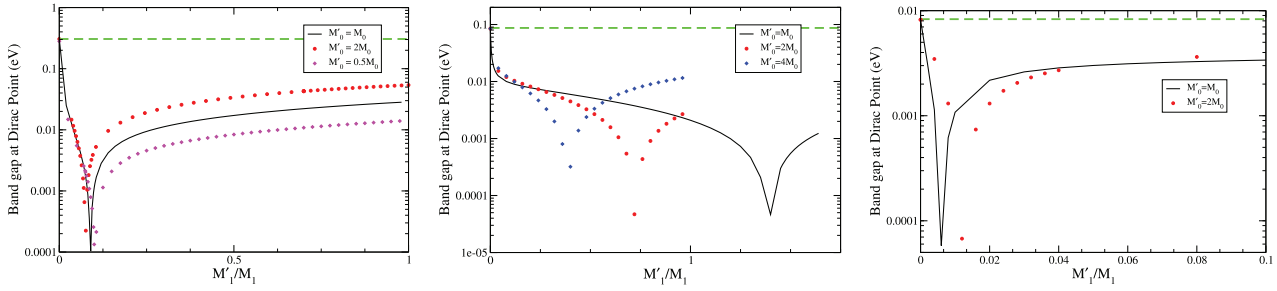

Figure A1. Band gap at the DP for the interface Hamiltonian for TI thickness of $L = 15$ Å (a) and $L = 20$ Å (b) $L = 30$ Å (c) as a function of the ratio of the band curvature of the CI and TI. The dashed horizontal green line in all the sub-figures indicates the value of band-gap for $M_1' = 0$ at the interface which is equivalent to an infinite wall at the boundary.

as a CI-TI-CI system where each of the layers is thick enough to assume that it is governed by the pure bulk Hamiltonians. If the TI layer is very thick, the Hamiltonian of Zhang *et al* [28] which is only valid in the long-wavelength limit (small k limit near the Γ point) is applicable. In this case we assume that the three layers are ideal layers governed by the ideal bulk Hamiltonians. The boundary condition for the wavefunction at the interface is found by integrating the Schrödinger equation along an infinitesimal region which encloses the interface.

A.1. Boundary conditions at the interface

We consider similar heterostructure as in the main text where the CI Hamiltonian extends $-\infty$ to $-(n+1)$ and $(n+1)$ to ∞ and the TI Hamiltonian extends from $-n+1$ to $n-1$ sites. The sites $\pm n$ are considered to be the boundary sites.

For completeness, we write the TI and the CI Hamiltonian in equations (A.1) and (A.2).

$$\hat{H}_{\rm TI}(z,\vec{k}_\perp) = (-M_0 - M_1\frac{\partial^2}{\partial z^2} + M_2 k_\perp^2)\Gamma_5 - iB_0\Gamma_4\frac{\partial}{\partial z} + A_0(\Gamma_1 k_y - \Gamma_2 k_x) \quad \text{(A.1)}$$

and the CI Hamiltonian is

$$\hat{H}_{\rm CI}(z,\vec{k}_\perp) = (M_0' - M_1'\frac{\partial^2}{\partial z^2} + M_2' k_\perp^2)\Gamma_5 - iB_0'\Gamma_4\frac{\partial}{\partial z} + C_0 I. \quad \text{(A.2)}$$

First, we write the BC at the left interface $z = z_1 = -na$. The first BC is trivial which follows from the continuity of the wavefunction, i.e.

$$\psi(z=0) = \psi(z = z_1 + 0). \quad \text{(A.3)}$$

For the second BC, we integrate the Schrödinger Equation $\hat{H}\psi(z) = E\psi(z)$, from $z = z_1 - \delta$ to $z = z_1 + \delta$ where $\hat{H} = \hat{H}_{CI}(z)$ for $z < z_1$ and $\hat{H} = \hat{H}_{TI}(z)$ for $z > z_1$, i.e.

$$\int_{z_1-\delta}^{z_1+\delta} {\rm d}z\hat{H}\psi(z) = E\int_{z_1-\delta}^{z_1+\delta} {\rm d}z\psi(z) \quad \text{(A.4)}$$

for infinitesimal δ. This gives the following relationship between the derivatives at the boundary:

$$\psi'(z_1+0)) = \frac{M_1'}{M_1}\psi'(z_1-0) + {\rm i}\frac{B_0' - B_0}{M_1}\Gamma_5^{-1}\Gamma_4\psi(z_1). \quad \text{(A.5)}$$

For simplification, we take $B_0' = B_0$, thus,

$$\psi'(z_1+0)) = \frac{M_1'}{M_1}\psi'(z_1-0) \quad \text{(A.6)}$$

which gives derivative discontinuity condition at the boundary. Similarly, the boundary condition at the other boundary at $z_2 = na$ is the following:

$$\psi'(z_2+0)) = \frac{M_1}{M_1'}\psi'(z_2-0). \quad \text{(A.7)}$$

A.2. Solving on the lattice

We write the wave-function at site $z = ma$ as a four component vector , $\psi_m = (\alpha_m, \beta_m, \gamma_m, \delta_m)$ in the spin-pseudospin basis $|\sigma,\tau\rangle$, i.e. in the following order: $\alpha_m = \langle\psi_m|\uparrow,+\rangle$, $\beta_m = \langle\psi_m|\uparrow,-\rangle$, $\gamma_m = \langle\psi_m|\downarrow,+\rangle$, $\delta_m = \langle\psi_m|\downarrow,-\rangle$. Then, the Hamiltonian on a descretized lattice for $m \leqslant -n-1$ as well as for $m \geqslant n+1$ (i.e. on the CI sides, with the exception of the boundary site $-n$) is as follows

$$(M_0' + M_2' k_\perp^2 + C_0)\Gamma_5\psi_m - \frac{iB_0}{2a}\Gamma_4(\psi_{m+1} - \psi_{m-1}) - \frac{M_1'}{a^2}\Gamma_5(\psi_{m+1} + \psi_{m-1} - 2\psi_m) = E\psi_m. \quad \text{(A.8)}$$

Similarly, for $-n+1 \leqslant m \leqslant n-1$ (i.e. on the TI side with the exception of the boundary site $-n$)

$$(-M_0 + M_2 k_\perp^2)\Gamma_5\psi_m + \frac{B_0}{2a}\Gamma_4(\psi_{m+1} - \psi_{m-1}) - \frac{M_1}{a^2}\Gamma_5(\psi_{m+1} + \psi_{m-1} - 2\psi_m) + A_0(\Gamma_1 k_y - i\Gamma_2 k_x)\psi_m = E\psi_m. \quad \text{(A.9)}$$

We get similar equations as in equations (A.8) and (A.9) for the other boundary.

The above constitutes $4(N-2)$ equations (N is the total number of sites), but there are $4N$ unknowns. This is because the above equations are for all other sites except the 2 boundary sites, $-n$ and $+n$ for the left and the right interface in this sandwich geometry. We include the following 4 boundary conditions for the left and the right interface which follows from the wavefunction derivative discontinuity at the boundary found in equations (A.6) and (A.7).

$$\psi_{-n} = \frac{M_1'\psi_{-n-1} + M_1\psi_{-n+1}}{(M_1' + M_1)} \quad \text{(A.10)}$$

$$\psi_{n} = \frac{M_1'\psi_{n-1} + M_1\psi_{n+1}}{(M_1' + M_1)} \quad \text{(A.11)}$$

Substituting for the value of $\psi_{\pm n}$ in equations (A.8) and (A.9) gives $4(N-2)$ eigen-value equations.

A.3. Results

In this section, we investigate the change in the band-gap of the interface Dirac cone of our heterostructure as a function of the CI parameters which is similar to our investigations in the main text for this BC. In figure A1, we plot the variation of the band-gap at the Dirac point (DP) as a function of the CI band-gap and band curvature parameters for different thickness of the TI in contact. We find that as a function of the ratio $r = \frac{M_1'}{M_1}$ the band-gap at the DP first decreases and then increases, thus, signaling a topological phase transition, i.e. if the initial phase is topological (hosts edge states), it becomes trivial and vice-versa. For example, in figure A1 (a), the heterostructure is initially in a trivial phase, i.e. it does not host any edge states. When $r > 0.1$, the system becomes topological. The exact value of r where such transition occurs depends on the thickness of the TI and the band-gap of the CI in contact.

ORCID iDs

Efstratios Manousakis https://orcid.org/0000-0002-6052-7790

References

[1] Zhang H, Liu C X, Qi X L, Dai X, Fang Z and Zhang S C 2009 *Nat. Phys.* **5** 438–42
[2] Xia Y *et al* 2009 *Nat. Phys.* **5** 398–402
[3] Fu L and Kane C L 2008 *Phys. Rev. Lett.* **100** 096407
[4] Zhang Q, Zhang Z, Zhu Z, Schwingenschlgl U and Cui Y 2012 *ACS Nano* **6** 2345–52
[5] Chang C Z, Tang P, Feng X, Li K, Ma X C, Duan W, He K and Xue Q K 2015 *Phys. Rev. Lett.* **115** 136801
[6] Eschbach M *et al* 2015 *Nat. Commun.* **6** 8816
[7] Cen C, Thiel S, Hammerl G, Schneider C, Andersen K, Hellberg C, Mannhart J and Levy J 2008 *Nat. Mater.* **7** 298
[8] Okamoto S and Millis A J 2004 *Nature* **428** 630
[9] Hasan M Z and Kane C L 2010 *Rev. Mod. Phys.* **82** 3045–67
[10] Jin H, Im J, Song J H and Freeman A J 2012 *Phys. Rev.* B **85** 045307
[11] Seixas L, West D, Fazzio A and Zhang S B 2015 *Nat. Commun.* **6** 7630
[12] Lee H and Yazyev O V 2017 *Phys. Rev.* B **95** 085304
[13] Jin K H, Yeom H W and Jhi S H 2016 *Phys. Rev.* B **93** 075308
[14] Freitas W A, Fazzio A and Schmidt T M 2016 *Appl. Phys. Lett.* **109** 131601
[15] Men'shov V N, Shvets I A, Tugushev V V and Chulkov E V 2017 *Phys. Rev.* B **96** 075302
[16] Shan W Y, Lu H Z and Shen S Q 2010 *New J. Phys.* **12** 043048
[17] Zhang Y *et al* 2010 *Nat. Phys.* **6** 584
[18] Liu W, Peng X, Wei X, Yang H, Stocks G M and Zhong J 2013 *Phys. Rev.* B **87** 205315
[19] Zhang T, Ha J, Levy N, Kuk Y and Stroscio J 2013 *Phys. Rev. Lett.* **111** 056803
[20] Tsipas P *et al* 2014 *ACS Nano* **8** 6614–9
[21] Chae J *et al* 2019 *ACS Nano* **13** 3931–9
[22] Liu C X, Zhang H, Yan B, Qi X L, Frauenheim T, Dai X, Fang Z and Zhang S C 2010 *Phys. Rev.* B **81** 041307
[23] Linder J, Yokoyama T and Sudbø A 2009 *Phys. Rev.* B **80** 205401
[24] Sakamoto Y, Hirahara T, Miyazaki H, Kimura S I and Hasegawa S 2010 *Phys. Rev.* B **81** 165432
[25] Lu H Z, Shan W Y, Yao W, Niu Q and Shen S Q 2010 *Phys. Rev.* B **81** 115407
[26] Kotulla M and Zlicke U 2017 *New J. Phys.* **19** 073025
[27] Deb O, Soori A and Sen D 2014 *J. Phys.: Condens. Matter* **26** 315009
[28] Liu C X, Qi X L, Zhang H, Dai X, Fang Z and Zhang S C 2010 *Phys. Rev.* B **82** 045122
[29] Fu L and Kane C L 2007 *Phys. Rev.* B **76** 045302
[30] Enaldiev V V, Zagorodnev I V and Volkov V A 2015 *JETP Lett.* **101** 89–96